



This is the post-print, accepted version of this article.

Frost, Ray L. and Xi, Yunfei and He, Hongping (2010) *Synthesis, characterization of palygorskite supported zero-valent iron and its application for methylene blue adsorption*. *Journal of Colloid and Interface Science*, 341. pp. 153-161. (In Press)

© Copyright 2009 Elsevier Inc. All rights reserved

1 **Synthesis, characterization of palygorskite supported zero-valent**
2 **iron and its application for methylene blue adsorption**

3
4 **Ray L. Frost ^{a,*}, Yunfei Xi ^{a,b,c}, Hongping He ^{a,d}**

5
6 *^a Inorganic Materials Research Program, School of Physical and Chemical Sciences,*
7 *Queensland University of Technology, GPO Box 2434, 2 George Street, Brisbane,*
8 *Qld 4001, Australia;*

9
10 *^b CERAR—Centre for Environmental Risk Assessment and Remediation, University of*
11 *South Australia, Mawson Lakes, SA 5095, Australia;*

12
13 *^c Cooperative Research Centre for Contamination Assessment and Remediation of the*
14 *Environment (CRC CARE), University of South Australia, Mawson Lakes, SA 5095,*
15 *Australia;*

16
17 *^d Guangzhou Institute of Geochemistry, Chinese Academy of Sciences, Wushan,*
18 *Guangzhou 510640, China*

19
20 **Corresponding Author:**

21
22 **Ray L. Frost**

23 **E: r.frost@qut.edu.au**

24 **P: +61 7 3138 2407**

25 **F: +61 7 3138 1804**

26

* Email address of corresponding author: r.frost@qut.edu.au

27 **Synthesis, characterization of palygorskite supported zero-valent**
28 **iron and its application for methylene blue decolourisation**

29

30 **Ray L. Frost**^{a,*}, **Yunfei Xi**^{a,b,c}, **Hongping He**^{a,d}

31

32 *^a Inorganic Materials Research Program, School of Physical and Chemical Sciences,*
33 *Queensland University of Technology, GPO Box 2434, 2 George Street, Brisbane, Qld*
34 *4001, Australia;*

35

36 *^b CERAR—Centre for Environmental Risk Assessment and Remediation, University of*
37 *South Australia, Mawson Lakes, SA 5095, Australia;*

38

39 *^c Cooperative Research Centre for Contamination Assessment and Remediation of the*
40 *Environment (CRC CARE), University of South Australia, Mawson Lakes, SA 5095,*
41 *Australia;*

42

43 *^d Guangzhou Institute of Geochemistry, Chinese Academy of Sciences, Wushan,*
44 *Guangzhou 510640, China*

45

46

* Email address of corresponding author: r.frost@qut.edu.au

47

48 **Abstract**

49

50 In this work, natural palygorskite impregnated with zero-valent iron (ZVI) was
51 prepared and characterised. The combination of ZVI particles on surface of fibrous
52 palygorskite can help to overcome the disadvantage of ultra-fine powders which may
53 have strong tendency to agglomerate into larger particles, resulting in an adverse
54 effect on both effective surface area and catalyst performance. There is a significant
55 increase of methylene blue (MB) decolourized efficiency on acid treated palygorskite
56 with ZVI grafted, within 5 mins, the concentration of MB in the solution was
57 decreased from 94 mg/L to around 20 mg/L and the equilibration was reached at
58 about 30 to 60 mins with only around 10 mg/L MB remained in solution. Changes in
59 the surface and structure of prepared materials were characterized using X-ray
60 diffraction (XRD), infrared (IR) spectroscopy, surface analysing and scanning
61 electron microscopy (SEM) with element analysis and mapping. Comparing with
62 zero-valent iron and palygorskite, the presence of zero-valent iron reactive species on
63 the palygorskite surface strongly increases the decolourization capacity for methylene
64 blue, and it is significant for providing novel modified clay catalyst materials for the
65 removal of organic contaminants from waste water.

66

67 **Keywords:** zero-valent iron, sepiolite, attapulgite, palygorskite, XRD, SEM, EDX,
68 infrared spectroscopy, adsorption-desorption, methylene blue.

69

70

71 **1. Introduction**

72 Organic contaminants in the environment especially in water have become a
73 major concern due to their toxicity. To remediate this pollution problem, various
74 chemical, physical and biological processes have been developed, such as microbial
75 degradation, filtration, adsorption, coagulation and membrane separation and others.
76 However, all these remediation methods have suffered from certain limitations and
77 disadvantages such as high cost, poor removal efficiency and possibility of desorption.
78 Thus, in recent years, reactions involving catalytic materials are becoming a more
79 ideal way which will degrade organic contaminants to completely harmless final
80 products. In the last decade, zero-valent iron (ZVI) has been increasingly used in
81 ground water remediation and hazardous waste treatment.

82

83 Laboratory studies have demonstrated that ZVI can effectively transform
84 chlorinated solvents, organochlorine pesticides, PCBs, organic dyes and heavy metals
85 [1-5]. These zero-valent iron (ZVI) materials were proposed as a reactive material in
86 permeable reactive barriers (PRBs) due to its great ability in reducing and stabilizing
87 different types of pollutants [6-8]. It has many advantages, such as nontoxic, as iron is
88 abundant in nature, lower price and high activity. This material with particle size at
89 the nano-scale exhibits superior activity because of their larger surface area and
90 higher reactivity [1]. However, similar to other nano-materials, this ultra-fine powder
91 has a strong tendency to agglomerate into larger particles, resulting in an adverse
92 effect on both effective surface area and catalyst performance; while another
93 disadvantage of this material is the separation and recovery of the fine particles after
94 usage. Using a support material for nano-sized ZVI is one possible way to solve this
95 problem. As reported in the literature, there are very few ZVI supported on inorganic
96 clay minerals [9]. Clays as abundant natural resources are suitable candidates to work
97 as supporting materials due to their inexpensiveness, availability, environmental
98 stability and high surface area/sorption capacity and ion exchange properties; their
99 sorption capacity attracts contaminants to the surface and thus enhances the
100 efficiency.

101

102 In this study, a PF1-1 palygorskite was investigated as a supporting material
103 for ZVI. This class of clay minerals is characterized by porous crystalline structures
104 containing tetrahedral layers alloyed together by longitudinal side chains [10, 11]. It is

105 a 2:1 type clay mineral which possesses moderate high structural charge due to
106 considerable substitution of Al^{3+} by Mg^{2+} and Fe^{2+} in the octahedral sheet [12]. In
107 addition, this clay mineral displays fibrous particle shape, fine particle size with
108 internal channels and moderate surface area [13].

109

110 A series of tests were carried out to characterise the surface properties of the
111 prepared ZVI materials. In addition, usually ZVI was used for degradation of
112 chlorinated compounds, in this study, this material was extended to methylene blue
113 removal and the removal ability was evaluated in the laboratory. Comparing with ZVI
114 and unmodified palygorskite, palygorskite supported ZVI showed much higher
115 efficiency for methylene blue removal with very small amount of ZVI supported. In
116 this study, scanning electron microscopy (SEM) with EDX together with other
117 characterization methods such as XRD, surface analysing and FTIR have been applied
118 for better understanding of the materials' structures and methylene blue removal
119 mechanisms.

120

121 **2. Experimental**

122

123 **2.1. Materials**

124 The palygorskite used in this study was supplied by the Clay Minerals Society
125 as source clay PF1-1 (palygorskite). This clay originates from Gadsden County, State
126 of Florida, USA. The chemical composition of the clay is 60.9% SiO_2 , 10.4% Al_2O_3 ,
127 0.49% TiO_2 , 2.98% Fe_2O_3 , 0.40% FeO , 0.058% MnO , 10.2% MgO , 1.98% CaO ,
128 0.058% Na_2O , 0.80% K_2O , 0.542% F , 0.80% P_2O_5 and 0.11% S . The formula of the
129 palygorskite can be expressed as $(\text{Ca}_{0.12} \text{Na}_{0.32} \text{K}_{0.05}) [\text{Al}_{3.01} \text{Fe(III)}_{0.41} \text{Mn}_{0.01} \text{Mg}_{0.54}$
130 $\text{Ti}_{0.02}] [\text{Si}_{7.98} \text{Al}_{0.02}] \text{O}_{20}(\text{OH})_4$, as calculated from its chemical composition. The cation
131 exchange capacity (CEC) is 19.5 meq/100 g and surface area is 136.4 m^2/g . The clay
132 was acid activated using 5M HCl. Sodium borohydride (NaBH_4) 98.5%, Iron (II)
133 chloride tetrahydrate ($\text{FeCl}_2 \cdot 4\text{H}_2\text{O}$) 99% and Methylene blue (MB) were obtained
134 from Sigma-Aldrich, absolute ethanol and hydrogen chloride were with analytical
135 grade and used without purification. A reduced iron powder was obtained from Sigma
136 with a purity of 99%.

137

138 **2.2. Preparation of ZVI and ZVI impregnated palygorskite**

139 10g of Palygorskite was pre-treated by soaking in 200ml of 5M HCl at 60 °C
140 oven for about 48 hrs and then was washed several times with deionized (DI) water to
141 remove excess acid. A liquid phase reduction method was used for nZVI and nZVI
142 impregnated palygorskite. In a typical procedure of ZVI preparation, 16.02 g of
143 $\text{FeCl}_2 \cdot 4\text{H}_2\text{O}$ was dissolved in a mixture of absolute ethanol and de-ionised water (72
144 ml ethanol plus 18 ml H_2O), this mixture is denoted as solution A. while 9.15g of
145 NaBH_4 was dissolved in 300ml of H_2O to form 1M solution, denoted as solution B.
146 Then solution B was added drop by drop to solution A in a fume hood, the resulting
147 reaction can be expressed as $\text{Fe}^{2+} + 2\text{BH}_4^- + 6\text{H}_2\text{O} \rightarrow \text{Fe}^0 + 2\text{B}(\text{OH})_3 + 7\text{H}_2\uparrow$, black
148 particles of ZVI appeared and then the mixture was further stirred for 2hrs and the
149 iron powder was separated from the solution by centrifugation and the sediment
150 washed with 250ml ethanol and dried in a 50°C oven without air evacuation overnight.
151 The powder prepared was kept in vacuum desiccator before use. This laboratory
152 made ZVI was denoted as ZVI-L. ZVI impregnated palygorskite was prepared by a
153 similar procedure as reported [9] with following steps: (a) 16.02g of $\text{FeCl}_2 \cdot 4\text{H}_2\text{O}$ was
154 dissolved in mixture of absolute ethanol and deionized (DI) water (72 ml ethanol + 18
155 ml H_2O), (b) 4.5g of acid treated palygorskite was suspended in the solution, the
156 mixture was stirred using a magnetic stirrer overnight for fully exchange/sorption of
157 iron (II) ions on clay. (c) The mixture was centrifuged and washed several times to
158 remove excess iron (II) ions and then it was resuspended into 72 ml of ethanol + 18
159 ml H_2O . After that, 300 ml of 1 M borohydride was added drop by drop to the
160 solution and further mixing of 2 hrs was allowed following the addition of NaBH_4
161 solution; then the solid was centrifuged and washed three times with 120 ml of
162 ethanol and dried in 50 °C oven without air evacuation overnight, this palygorskite
163 supported ZVI was denoted as ZVI-P. As reported in the literature, using ethanol to
164 wash samples instead of water is critical in stabilizing ZVI against immediate
165 oxidation [1, 14], and drying in atmosphere oven has a passivation effect for ZVI
166 application which may otherwise catch fire on exposure to atmospheric oxygen [14].

167

168 **2.3. Characterisation methods**

169 The samples were pressed in stainless steel sample holders. X-ray diffraction
170 (XRD) patterns were recorded using $\text{CuK}\alpha$ radiation ($n = 1.5418\text{\AA}$) on a Panalytical
171 X'Pert (PW3040) diffractometer operating at 40 kV and 50 mA between 3 and 73° or
172 5 to 90° (2θ) at a step size of 0.0167°.

173

174 Infrared spectra were obtained using a Nicolet Nexus 870 FTIR spectrometer
175 with a smart endurance single bounce diamond ATR cell. Spectra over the 4000–550
176 cm^{-1} range were obtained by the co-addition of 64 scans with a resolution of 4 cm^{-1}
177 and a mirror velocity of 0.6329 cm/s.

178

179 Peakfit software package (AISN Software Inc.) was used to undertake band
180 component analysis that enabled the type of fitting function to be selected and
181 allowed specific parameters to be fixed or varied accordingly. Gauss–Lorentz cross-
182 product function with the minimum number of component bands was used for band
183 fitting. The fitting was undertaken until reproducible results were obtained with
184 squared correlations of r^2 greater than 0.98.

185

186 Adsorption and desorption experiments using N_2 were carried out at 77 K on a
187 TRISTAR 3000 surface analyser. Prior to each measurement the samples were
188 degassed at 353K for 24hrs. The N_2 isotherms were used to calculate the specific
189 surface area (SA) and the surface area was determined using multipoint BET method
190 [15]. An FEI QUANTA 200 scanning electron microscope (SEM) with integrated
191 energy dispersive X-ray analyser system was used for morphological studies, samples
192 were coated with carbon. A Philips CM 200 transmission electron microscope (TEM)
193 was used to investigate the microstructure of prepared nZVI.

194

195

196 **2.4. Methylene blue decolourization tests**

197 Methylene blue decolourization experiments were conducted at room
198 temperature (25 °C). In a typical experiment, 0.4 g of sample was mixed with 400 ml
199 of 100 ppm methylene blue solution at its natural pH. The solution was stirred for
200 certain period of time using a magnetic stirrer. At certain time intervals, about 4 ml of
201 liquid sample was removed by syringe and filtered using $0.45 \mu\text{m}$ PTFE syringe
202 filters, dye concentration was determined spectrophotometrically on an Varian Cary 3
203 UV-Visible Spectrophotometer by measuring absorbance at k_{max} of 665 nm for MB
204 [13]. The change of MB amount was calculated from the difference between the
205 initial and final/equilibrium solution concentrations; solid-phase loading of MB, q_e
206 (mg/g) was computed from the mass balance: $q_e = V(C_i - C_e)/M$; where, C_i and C_e are

207 total dissolved and equilibrium liquid phase concentration (mg/L), respectively, and
208 M is the dose of sorbent (g/L), V is the volume of the solution (mL). Blank
209 experiments were also performed using solutions without sorbent materials in order to
210 check any possible loss from sorption onto the surface of beaker/syringe/filters and
211 the results showed that the sorption onto surfaces were negligible. All working
212 solutions were prepared from MB stock solution diluted with deionized (DI) water
213 and all experiments were carried out in duplicate.

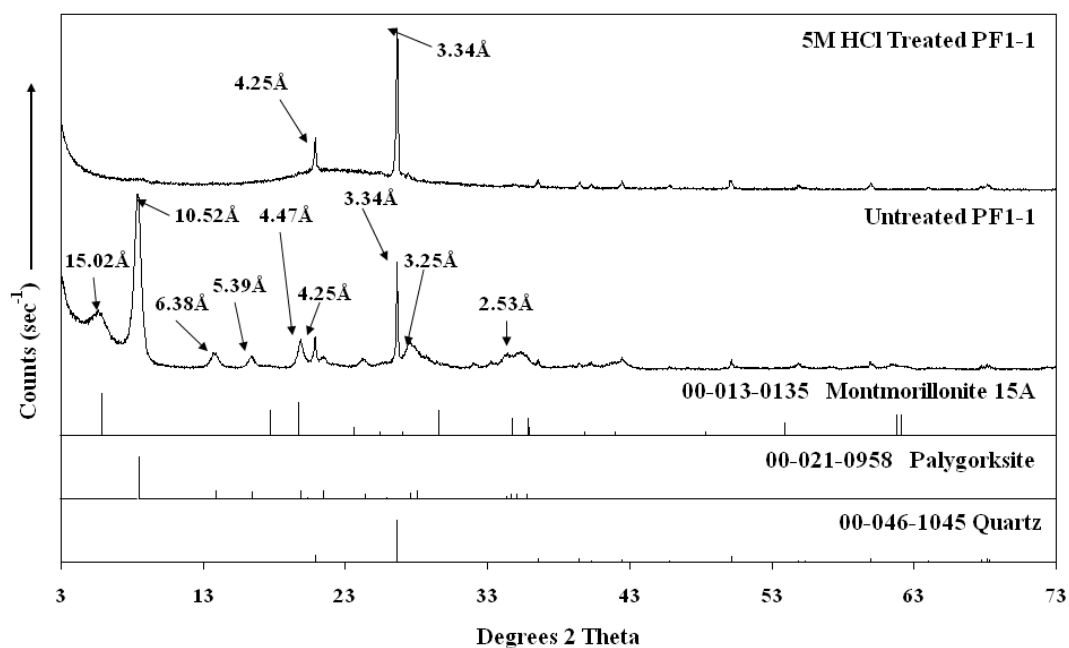
214

215 3. Results and discussion

216

217 3.1 Characterization results

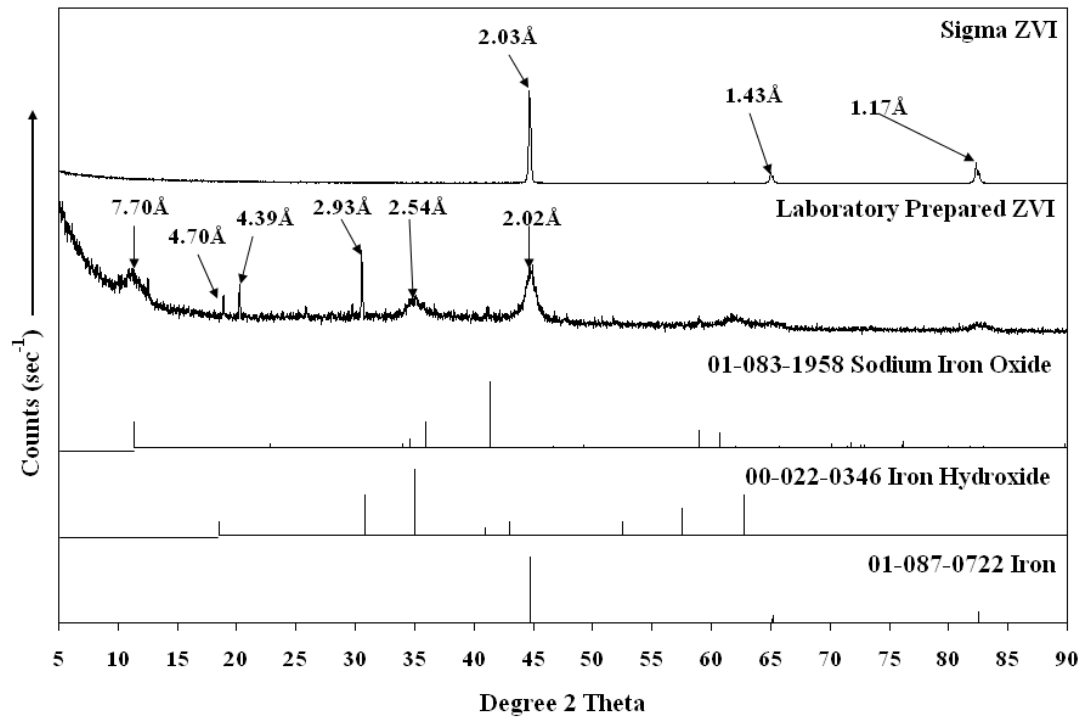
218



219

220 **Fig. 1a XRD patterns of untreated/acid treated palygorskite**

221

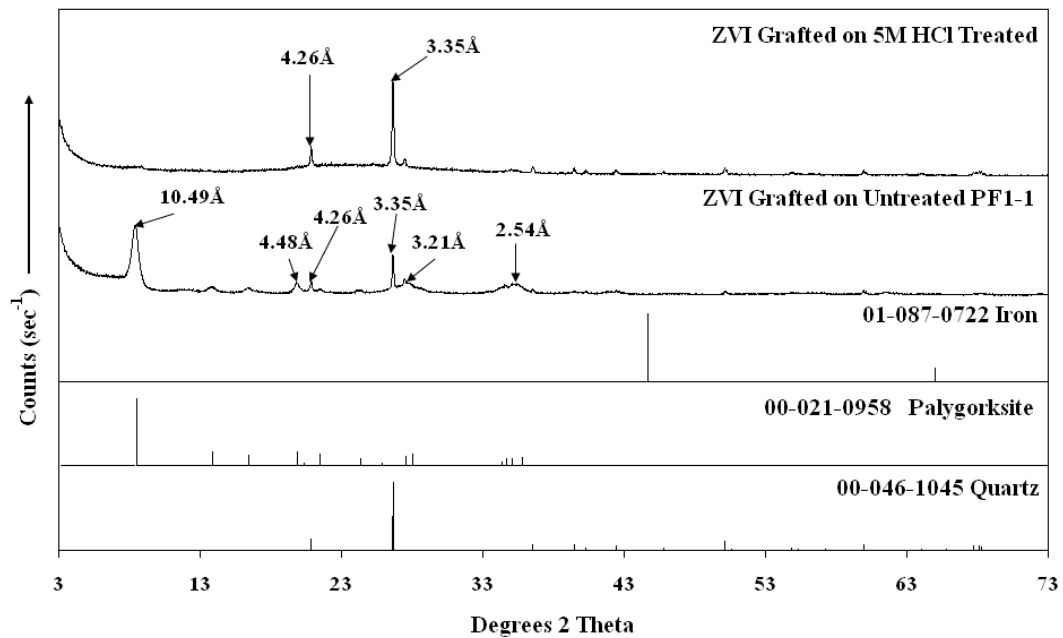


222

223 **Fig. 1b XRD patterns of lab made ZVI and ZVI from Sigma**

224

225



226

227 **Fig. 1c XRD patterns of ZVI grafted on untreated/acid treated palygorskite**

228

229

230

231 ***X-ray diffraction***

232 Fig. 1 shows the XRD patterns of untreated palygorskite, 5M HCl treated
233 palygorskite, palygorskite supported ZVI, ZVI from Sigma and laboratory made ZVI.
234 In case of the untreated palygorskite, powder XRD shows peaks that match the pattern
235 in the JCPDS standard 00-021-0958, the peak observed at 10.52 Å is prominent and
236 attributed to the (110) plane which comes from the large distance between neighbour
237 half-unit cells in the crystal structure. In addition, the relatively strong peaks at 4.25 Å,
238 4.47 Å and 3.69 Å represent the 040, 121 and 221 planes, respectively. While an
239 intense peak at 3.34 Å ($2\theta = 26.7^\circ$) is from a quartz impurity [16]. Other peaks at 6.38
240 Å, 5.39 Å, 3.25 Å and 2.53 Å were also observed for this PF1-1-palygorskite. After
241 this clay was treated with 5 M HCl, only peak at 4.25 Å and peak from quartz at 3.34
242 Å were observed. It is concluded that this acid treatment has changed the crystal
243 structure of palygorskite and this palygorskite is less stable under acid attack than
244 another palygorskite the results of which reported in a literature [17]. The XRD
245 patterns of laboratory synthesised ZVI and ZVI obtained from Sigma are shown in
246 Fig. 1b. Both ZVIs showed strong peaks at about 2.02 Å and 2.03 Å respectively
247 which is a characteristic reflection for ZVI [14]. And it also indicates that for ZVI
248 from Sigma, the iron is mainly in its Fe⁰ state (only characterised by the basic
249 reflection at 44.9° (2θ), however some oxides were observed in laboratory made ZVI
250 which showed peaks at 2.93 Å and 2.54 Å ascribed to lepidocrocite (γ-FeOOH) and
251 magnetite (Fe₃O₄)/ maghemite (γ-Fe₂O₃) respectively. Some researchers have
252 suggested a core-shell structure [18-20], where the iron nanoparticles form a core
253 composed of zero-valent iron with a shell of iron oxides. Because of surface
254 hydroxylation, FeOOH is also present [20]. Small peaks at about 1.43 Å and 1.17 Å
255 were also observed on both samples from iron which is in accordance with that
256 reported in a literature [21]. With ZVI grafted on untreated PF1-1 and 5M HCl treated
257 palygorskite as shown in Fig. 1c, no obvious iron peak at 2.02 Å was observed in both
258 cases and in both samples, the palygorskite peaks were well preserved. The absence
259 of strong iron peak may be due to the smaller amount of ZVI grafted on clays.

260
261
262
263
264

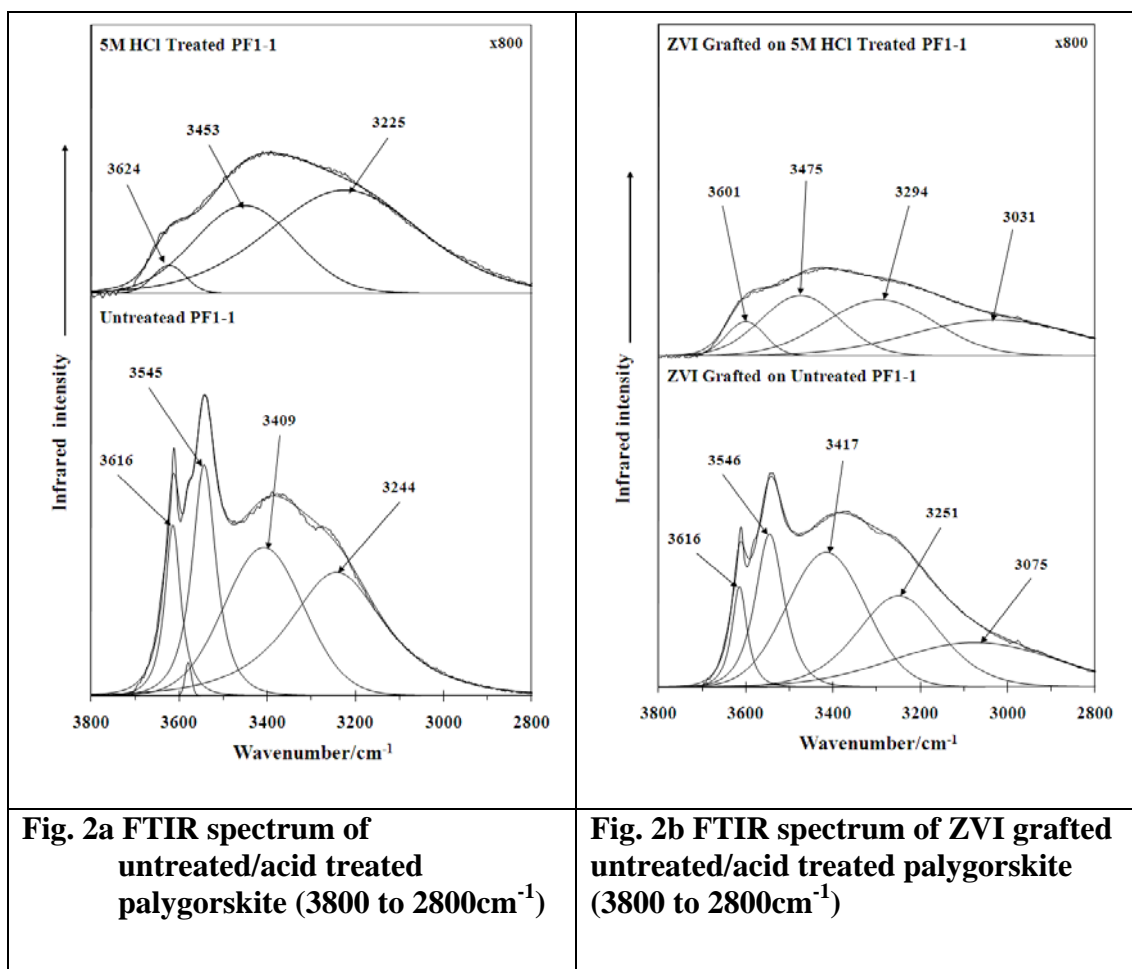
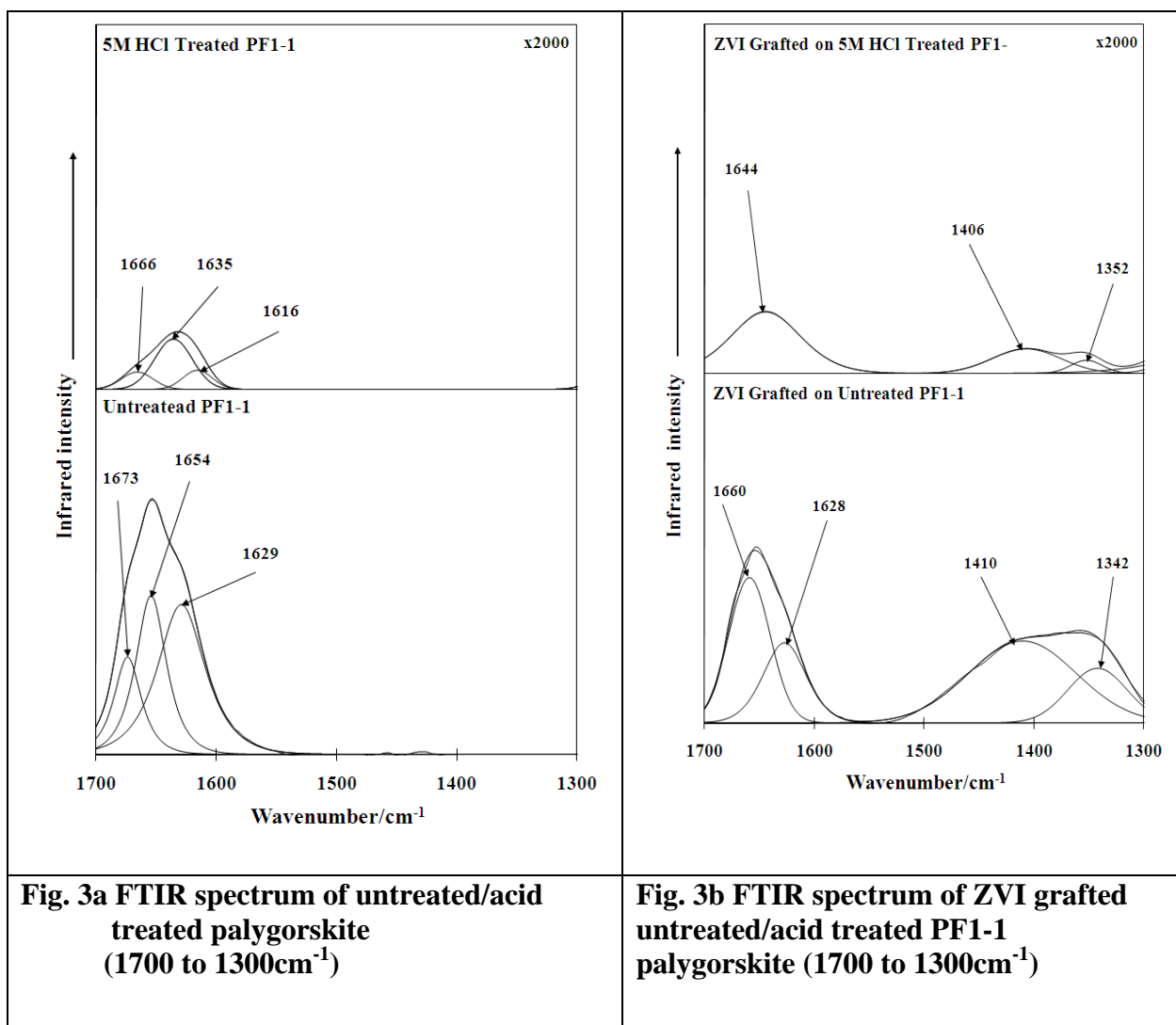


Fig. 2a FTIR spectrum of untreated/acid treated palygorskite (3800 to 2800 cm^{-1})

Fig. 2b FTIR spectrum of ZVI grafted untreated/acid treated palygorskite (3800 to 2800 cm^{-1})

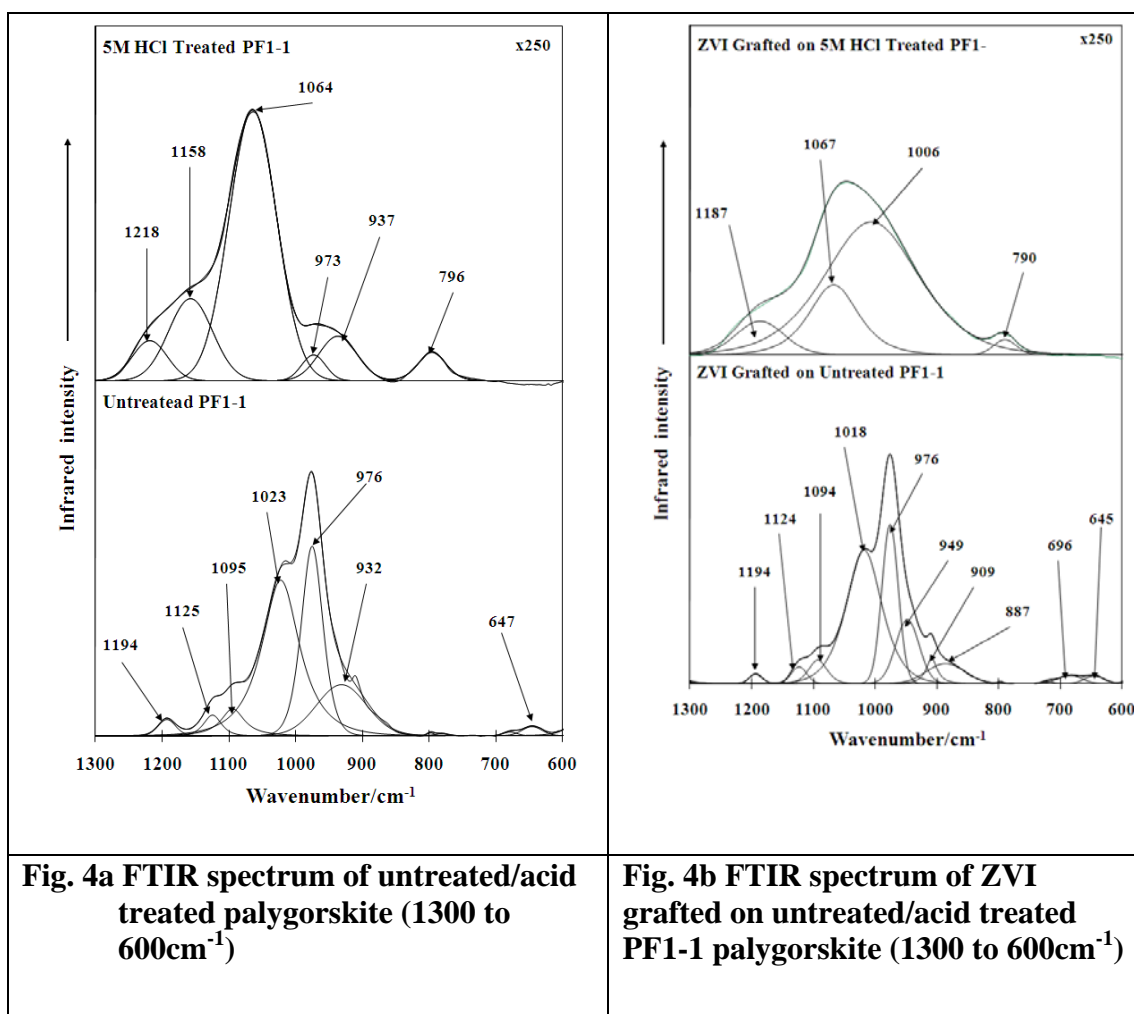
268 The infrared spectrum of the palygorskite clay, acid treated palygorskite and
 269 ZVI grafted samples may be divided into three sections: (a) 2800-3800 cm^{-1} (Figure
 270 2), (b) 1300-1700 cm^{-1} (Figure 3) and (c) 600-1300 cm^{-1} (Figure 4) for easier study.
 271 Fig. 2a shows the OH-stretching vibration region, the following peaks can be
 272 observed for untreated palygorskite: sharp peaks at 3616 cm^{-1} and 3545 cm^{-1} , a peak at
 273 3409 cm^{-1} and a shoulder at 3244 cm^{-1} , where the peak at 3616 cm^{-1} is a characteristic
 274 peak for palygorskite as described in many studies [22-25], corresponding to Al-Al-
 275 OH stretching band. This band shifts to 3624 cm^{-1} with less intensity after acid
 276 treatment, a tiny peak was observed at about 3580 cm^{-1} which is ascribed to
 277 coordinated water molecules in the channels of the palygorskite [25, 26] or Al-Fe-
 278 OH/Al-Mg-OH bonds [25, 27], while band at 3545 cm^{-1} is attributed to OH stretching
 279 vibration of water coordinated to Al, Mg [28]. A contribution of the OH stretching
 280 mode in Al-Mg-OH, Fe-Mg-OH and Fe-Fe-OH groups is also considered [25, 26].

281 The bands studied are similar in position and intensity after ZVI grafted on untreated
 282 palygorskite as shown in Fig. 2b. However after acid treatment, no matter with ZVI
 283 grafted or not, there are big differences of bands' position and intensity in this region
 284 as can be observed in Fig. 3a and Fig. 3b.
 285



286
 287 In the water-bending vibrational region, two partially resolved peaks at 1654
 288 cm⁻¹ and 1629 cm⁻¹ were observed as shown in Fig. 3a which correspond to bending
 289 modes of absorbed and zeolitic water and they are in accordance with the literature
 290 [29] which reported the presence of peaks at 1655 cm⁻¹ and 1630 cm⁻¹ respectively.
 291 Though peaks intensities changed significantly, however after acid treatment, the
 292 peaks positions in this region didn't change by a great deal. As shown in Fig. 4a, the
 293 peaks between 1200 cm⁻¹ and 600 cm⁻¹ are characteristic bands of silicate
 294 corresponding to tetrahedral sheet Si-O stretching modes and M-O deformation [23].

295 When the spectra of the samples are compared, some important differences can be
 296 found as significant differences in the peaks' intensities from untreated and 5M HCl
 297 treated palygorskites are observed, after acid treatment the peak intensities in this
 298 region was decreased dramatically. The first peak that appears in this region in all
 299 samples studied is located at 1194 cm^{-1} which is characteristic of palygorskite. This
 300 peak shifts to 1218 cm^{-1} after acid treatment. This peak only appears in palygorskite
 301 and sepiolite but not in lamellar clay minerals and is from Si-O-Si bond [24] between
 302 the alternative ribbons.
 303



304

305 The most intensive peaks observed in this region are at 1023 cm^{-1} and 976
 306 cm^{-1} respectively corresponding to stretching vibration of Si-O bond [30]. There are
 307 changes observed on these bands after acid treatment which may due to the
 308 dissolution of octahedral sheets, where the silicate sheets presumably convert to
 309 silanol groups [24]. The presence of small quantities of impurities can be clearly

310 detected in this spectrum, where quartz produced band at about 796 cm^{-1} [25, 28] and
311 this peak became relative stronger comparing with other peaks in this region after acid
312 treatment which showed quartz was resistance to acid treatment, and it also confirmed
313 the conclusion as obtained from XRD results. There are also several other bands
314 observed where one placed at about 647 cm^{-1} are related to bonds corresponding to
315 tetrahedral sheet. The shoulder at 676 cm^{-1} is related to the Mg content, after acid
316 treatment, these bands are not observed, which may due to the loss of Mg contents
317 after acid washing. And acid treated palygorskite showed quite some difference in
318 peaks position and intensity comparing with untreated one.

319

320 **BET adsorption-desorption**

321

322 Adsorption and desorption experiments using N_2 were carried out at 77 K. The
323 N_2 isotherms have been applied to calculate the specific surface area (SA) using
324 multipoint BET [15] method. It can be observed that acid treatment has increased the
325 surface area of palygorskite from $209.88\text{ m}^2/\text{g}$ to $277.62\text{ m}^2/\text{g}$ which is in accordance
326 with conclusion drawn in a literature [17]. And in literature, acid treatment showed
327 increased number of sorption sites toward metal ions on palygorskite, as this
328 procedure may disaggregate particles, eliminate impurities and increase surface area
329 of the clay [10, 31]. It also leads to partial leaching of magnesium, aluminium and
330 iron contents of palygorskite [32]. Preliminary results have shown that ZVI grafted on
331 acid treated palygorskite has better reactivity compared with grafted on untreated clay
332 (results not shown). ZVI purchased from Sigma only has a surface area at about 0.12
333 m^2/g , however laboratory prepared ZVI showed a surface area at $80.6\text{ m}^2/\text{g}$. It was
334 also observed that after ZVI grafting on acid treated palygorskite, the surface area
335 decreased from $277.6\text{ m}^2/\text{g}$ to $76.9\text{ m}^2/\text{g}$.

336

337

338

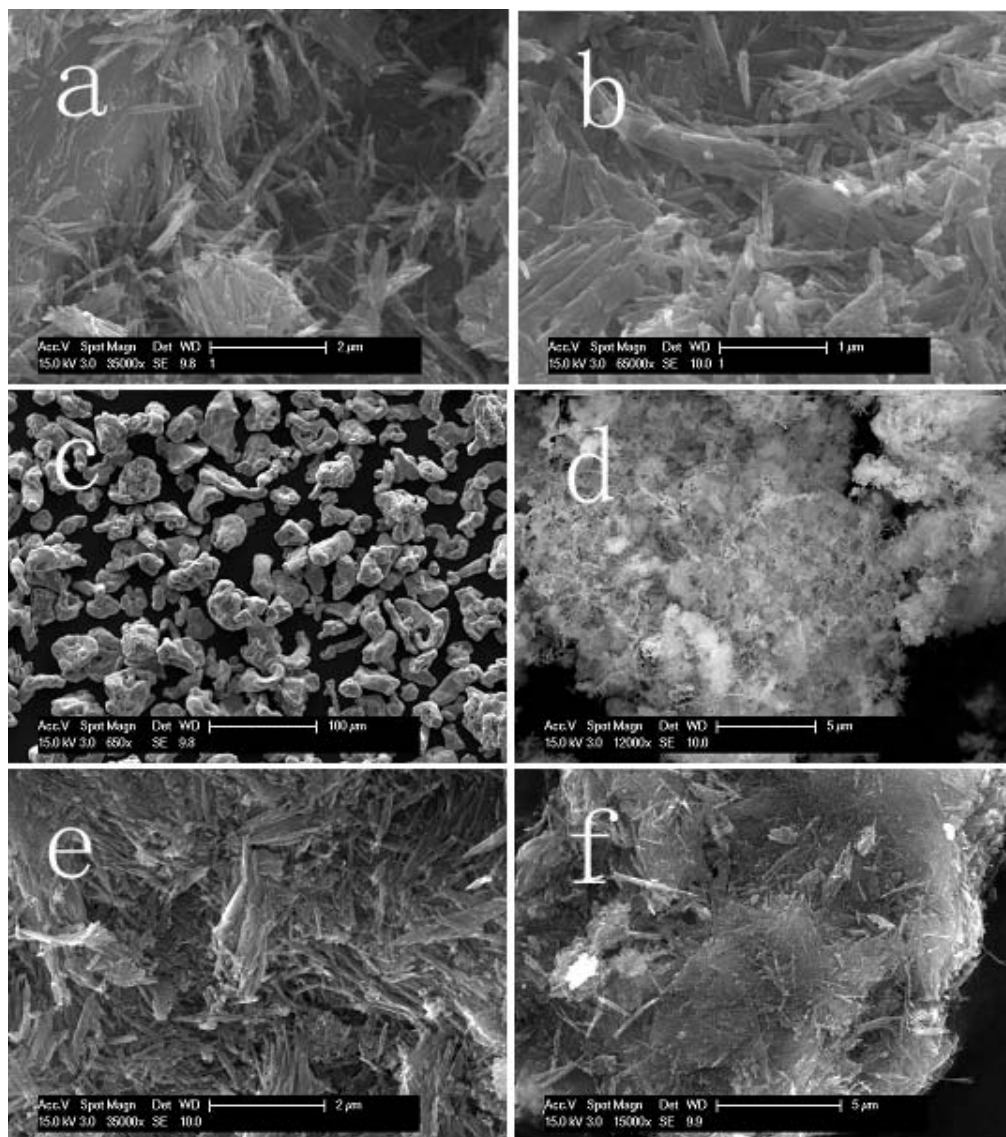
339

340

341

342

343



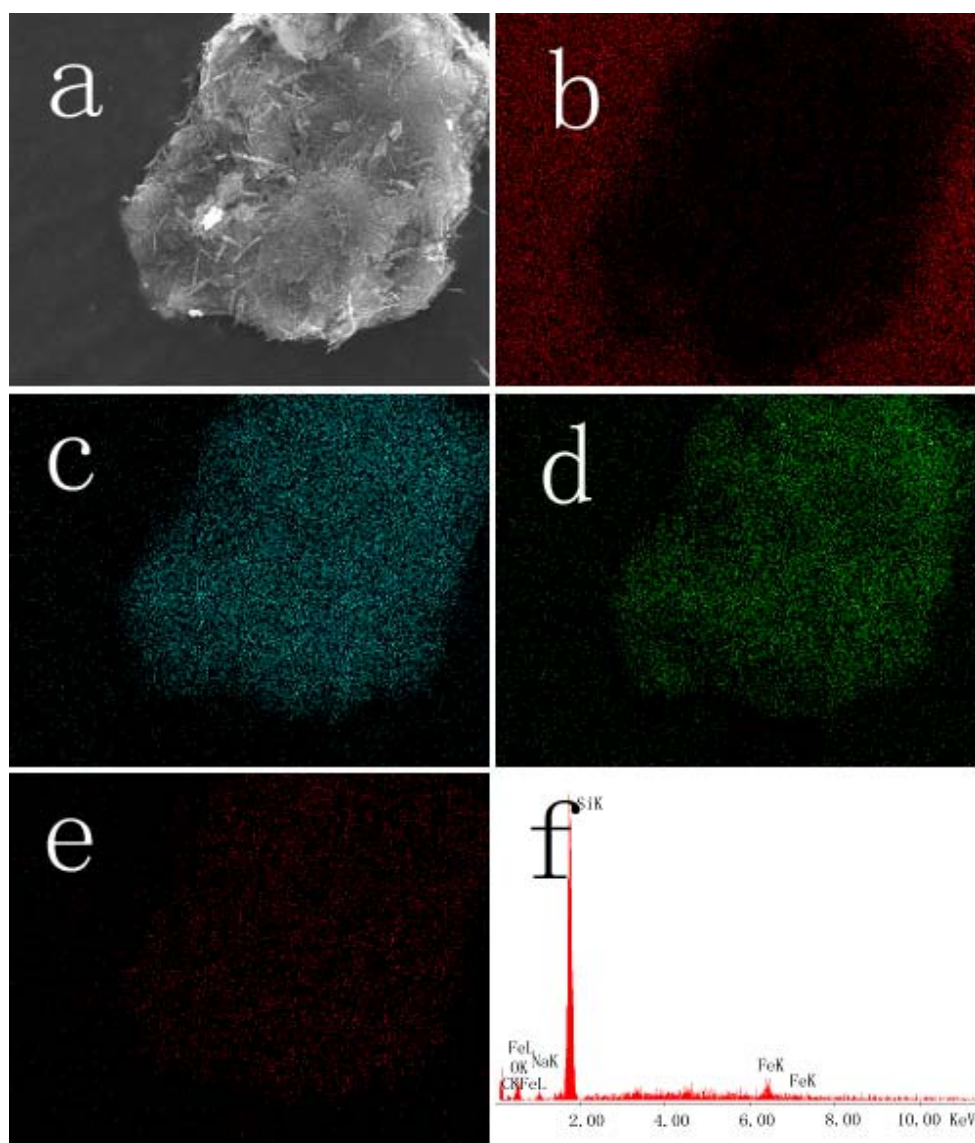
346

347 **Fig. 5 SEM images of a: untreated PF1-1 palygorskite; b: 5M HCl treated**
348 **palygorskite; c: ZVI from Sigma; d: laboratory made ZVI; e: ZVI grafted on**
349 **treated palygorskite and f: ZVI grafted on untreated palygorskite**

350

351 The SEM images of the palygorskite and its modified products are shown in
352 Figure 5. The unmodified palygorskite (Fig. 5a) shows bundles of close packed fibres
353 [33] or mat of tightly interwoven fibres [34], with variable thickness and length.
354 These fibres have flat or straight shapes and are oriented randomly in aggregates
355 similar to that observed in some other studies [11, 35]. Morphologic differences
356 between unmodified palygorskite and ZVI grafted palygorskite are not significant and
357 only textural features were observed on the surface of the clay which may due to the

358 iron particles after ZVI grafting. The SEM images of Sigma ZVI and laboratory
359 prepared ZVI are shown in Fig. 5c and 5d. The ZVI obtained from Sigma showed big
360 particles with sizes at around several tens of microns with irregular shapes (Fig. 5c).
361 The laboratory made iron particles (Fig. 5d) demonstrate the chain-like morphology
362 with floc aggregates similar to that observed in a study [1]. The morphology and size
363 difference of two kinds of ZVIs also illustrated the big differences on surface areas
364 obtained as discussed above. It is also likely that the ZVI has core-shell structures
365 where oxidised irons surround Fe(0) core and thus prevent it against further oxidation.
366 SEM in this study is also used to examine the changes in morphology of palygorskite
367 upon modification with ZVI.



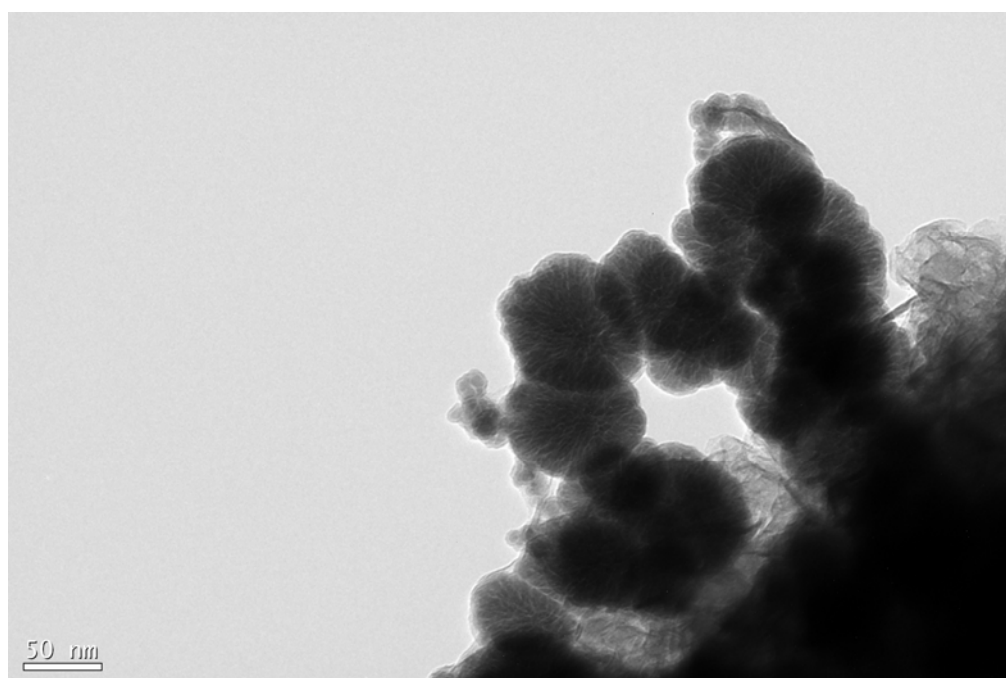
368
369

370 **Fig. 6 EDX mapping and element analysis on ZVI grafted palygorskite a: SEM**
371 **image; b: C element distribution; c: Si element distribution; d: O element**
372 **distribution; e: Fe element distribution and f: EDX spectrum of selected area**

373

374

375 EDX mapping and element analysis are shown in Figure 6. EDX element
376 analysing has demonstrated that after acid treatment, fewer amounts of magnesium
377 and aluminium were observed as shown in Fig. 6f, and a tiny peak from Fe was
378 shown in this figure which proves the successful grafting of ZVI on palygorskite
379 surface, and this peak was not observed in acid treated sample (figure not shown). The
380 EDX mappings of elements C, Si, O and Fe in a selected area of ZVI grafted
381 palygorskite are illustrated in Fig. 6b, Fig. 6c, Fig. 6d and Fig. 6e respectively where
382 even distribution of elements including Fe are present. This observation has also
383 confirmed the grafting of ZVI on clay surface. It is observed in TEM (Fig. 7) that the
384 chain-like laboratory made nZVI is composed of sphere shaped (but not regular)
385 particles as basic units, these ZVI particles have a size at around 80 nm in diameter.



386

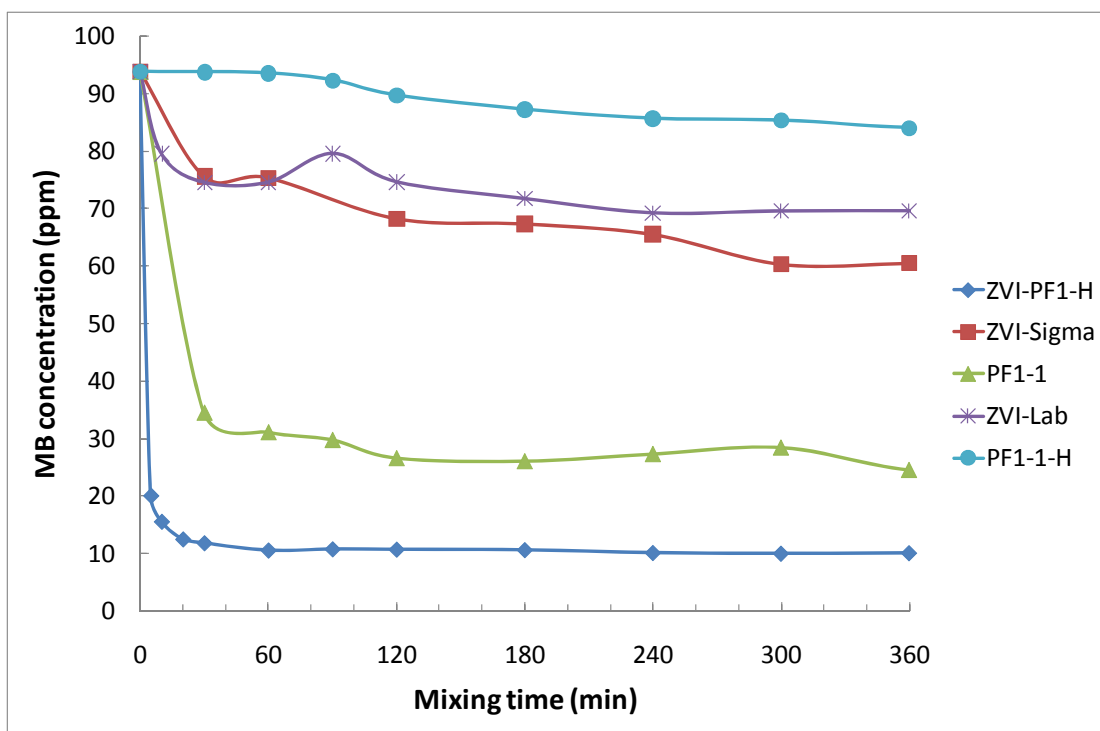
387 **Fig. 7 TEM image of laboratory made ZVI particles**

388

389

390 **3.2 MB decolourization results**

391



392
393 **Fig. 7 Effect of mixing time on MB removal**

394
395 For optimising decolourization time, at natural pH of 5.9, a set of experiments
396 has been performed equilibrating 400 mL of approximate 100 mg/L MB solution with
397 0.4 g of different materials. The suspensions were usually shaken at 25 °C for certain
398 period of time (5, 10, 30, 60, 90, 120, 180, 240, 300mins and up to 360mins), then the
399 dye concentration has been measured to calculate MB concentration remained in
400 solution. Fig. 8 shows the time dependent MB decolourization curve for all the
401 investigated samples. It can be seen that among all the samples, acid treated
402 palygorskite can absorb least amount of MB and within the first 60 mins, only
403 negligible amount was adsorbed. Even up to 360 mins, the concentration of MB was
404 only decreased from 94 mg/L to 84 mg/L (10.4% absorbed), and its performance is
405 even worse comparing with that of unmodified palygorskite where there is an obvious
406 decrease of MB concentration within 30 mins with 34.5 mg/L left in the solution and
407 afterwards the concentration was further decreased to about 24-26 mg/L, this
408 demonstrates that MB which has positive charged groups can be absorbed by
409 negatively charged clay surface. As for laboratory made ZVI and ZVI obtained from
410 Sigma, with increase of contact time, the amount of MB removed was increased
411 steadily and the decolourization capacities for both samples are comparable and
412 concentrations lower than 75 mg/L was reached within 30 mins and then it was

413 decreased to 69-60 mg/L until 360 mins of contact time. Generally, lab made ZVI can
414 decolour slightly higher amount of MB than that purchased from Sigma, it may
415 because lab made ZVI has much higher surface area at about 80.6 m²/g comparing
416 with that obtained from Sigma with a surface area only at 0.12 m²/g, the morphology
417 differences between these two ZVIs are also the possible reason to interpret the higher
418 activity obtained on lab made ZVI.

419

420 There is a significant increase of MB decolourized efficiency on acid treated
421 palygorskite with ZVI grafted, within 5 mins, the concentration of MB in the solution
422 was decreased from 94 mg/L to around 20 mg/L and the equilibration was reached at
423 about 30 to 60 mins with only around 10 mg/L MB remained in the solution. It is
424 apparent that modification of palygorskite with ZVI can increase the sorption capacity
425 comparing with only ZVI or palygorskite. The decolourization mechanism can be the
426 reduction of MB to leukomethylene blue (LMB) by ZVI species and the adsorption of
427 MB directly on ZVI surface, but as ZVI grafted palygorskite showed better results
428 comparing with ZVI only, adsorption of MB may not be the most important factor.
429 But it is more likely that co-precipitation with in-situ generated corrosion products
430 can be the main reason which could interpret the uptake of MB from solution as
431 discussed in some studies [36]. And the Fe(0) on clay surface could corrode more
432 rapidly, especially when these particles are well distributed on the surface of acid
433 activated palygorskite, thereby showed significant higher activity in the MB
434 decolourization than only on ZVI or clay. Further work will be needed to optimize the
435 MB decolourization procedure.

436

437 **4. Conclusions**

438

439 Zero valent iron (ZVI) and ZVI grafted palygorskite were prepared using
440 reduction methods and these materials together with untreated/acid treated
441 palygorskite, ZVI purchased from Sigma have been applied for methylene blue
442 decolourization. It was observed that ZVI grafted palygorskite has increased
443 decolourization capacity on MB comparing with that of ZVI or untreated palygorskite,
444 and co-precipitation on in-situ generated corrosion iron products was probably the
445 main reason explaining the uptake of MB from the studied solutions. In this study, X-
446 ray diffraction patterns were obtained for these materials; peaks from different planes

447 diffractions were illuminated and quartz was determined as a main impurity, it was
448 observed that the acid treatment has changed the crystal structure of palygorskite.
449 Comparing with ZVI obtained from Sigma which has mainly iron phase, laboratory
450 made ZVI showed phases from iron oxides. SEM studies showed different
451 morphology between these two ZVIs, the structural information of palygorskite and
452 ZVI grafted ones were also obtained and discussed. EDX element mapping was
453 proven to be a useful tool illustrating the distribution of elements, and iron phase
454 though not detected by XRD, was observed evenly distributed on the clay surface by
455 this technique. Infrared ATR techniques were used to study the changes in the bands
456 positions of palygorskite upon acid treatment and ZVI grafting, changes in both the
457 wavenumber and the intensity of the bands were observed after acid treatment and
458 grafting. The result is very important for the application of ZVI grafted natural clays
459 for the decolourization of organic dyes from waste water.

460

461 **Acknowledgements**

462 The financial and infra-structure support of the Queensland University of
463 Technology Inorganic Materials Research Program of the School of Physical and
464 Chemical Sciences is gratefully acknowledged. The Australian Research Council
465 (ARC) is thanked for funding the instrumentation

466

467 **References**

468

- 469 1. C. Uzum, et al., *Application of zero-valent iron nanoparticles for the removal*
470 *of aqueous Co²⁺ ions under various experimental conditions*. Chemical
471 Engineering Journal, 2008. **144**(2): p. 213-220.
- 472 2. Cantrell, K.J., D.I. Kaplan, and T.W. Wietsma, *Zero-valent iron for the in situ*
473 *remediation of selected metals in groundwater*. Journal of Hazardous
474 Materials, 1995. **42**(2): p. 201-212.
- 475 3. Cho, H.-H. and J.-W. Park, *Sorption and reduction of tetrachloroethylene with*
476 *zero valent iron and amphiphilic molecules*. Chemosphere, 2006. **64**(6): p.
477 1047-1052.
- 478 4. Dombek, T., et al., *Rapid reductive dechlorination of atrazine by zero-valent*
479 *iron under acidic conditions*. Environmental Pollution, 2001. **111**(1): p. 21-27.

- 480 5. Ghauch, A., et al., *Rapid treatment of water contaminated with atrazine and*
481 *parathion with zero-valent iron*. Chemosphere, 1999. **39**(8): p. 1309-1315.
- 482 6. Scherer, M.M., et al., *Chemistry and Microbiology of Permeable Reactive*
483 *Barriers for In Situ Groundwater Clean up*. Critical Reviews in
484 Environmental Science and Technology, 2000. **30**(3): p. 363-411.
- 485 7. Cundy, A.B., L. Hopkinson, and R.L.D. Whitby, *Use of iron-based*
486 *technologies in contaminated land and groundwater remediation: A review*.
487 Science of The Total Environment. **In Press, Corrected Proof**.
- 488 8. Ahn, J.S., et al., *Arsenic removal using steel manufacturing byproducts as*
489 *permeable reactive materials in mine tailing containment systems*. Water
490 Research, 2003. **37**(10): p. 2478-2488.
- 491 9. Uzum, C., et al., *Synthesis and characterization of kaolinite-supported zero-*
492 *valent iron nanoparticles and their application for the removal of aqueous*
493 *Cu²⁺ and Co²⁺ ions*. Applied Clay Science. **In Press, Corrected Proof**.
- 494 10. Chen, H., Y. Zhao, and A. Wang, *Removal of Cu(II) from aqueous solution by*
495 *adsorption onto acid-activated palygorskite*. Journal of Hazardous Materials,
496 2007. **149**(2): p. 346-354.
- 497 11. Aiban, S.A., *Compressibility and swelling characteristics of Al-Khobar*
498 *Palygorskite, eastern Saudi Arabia*. Engineering Geology, 2006. **87**(3-4): p.
499 205-219.
- 500 12. Polette-Niewold, L.A., et al., *Organic/inorganic complex pigments: Ancient*
501 *colors Maya Blue*. Journal of Inorganic Biochemistry, 2007. **101**(11-12): p.
502 1958-1973.
- 503 13. Al-Futaisi, A., A. Jamrah, and R. Al-Hanai, *Aspects of cationic dye molecule*
504 *adsorption to palygorskite*. Desalination, 2007. **214**(1-3): p. 327-342.
- 505 14. Celebi, O., et al., *A radiotracer study of the adsorption behavior of aqueous*
506 *Ba²⁺ ions on nanoparticles of zero-valent iron*. Journal of Hazardous
507 Materials, 2007. **148**(3): p. 761-767.
- 508 15. Brunauer, S., P.H. Emmett, and E. Teller, *Adsorption of gases in*
509 *multimolecular layers*. Journal of the American Chemical Society, 1938. **60**: p.
510 309-19.
- 511 16. Post, J.L. and S. Crawford, *Varied forms of palygorskite and sepiolite from*
512 *different geologic systems*. Applied Clay Science, 2007. **36**(4): p. 232-244.

- 513 17. Corma, A., A. Mifsud, and E. Sanz, *Influence of the chemical composition and*
514 *textural characteristics of palygorskite on the acid leaching of octahedral*
515 *cations*. Clay Minerals, 1987. **22**(2): p. 225-32.
- 516 18. Nurmi, J.T., et al., *Characterization and Properties of Metallic Iron*
517 *Nanoparticles: Spectroscopy, Electrochemistry, and Kinetics*. Environmental
518 Science and Technology, 2005. **39**(5): p. 1221-1230.
- 519 19. Liu, Y., et al., *Trichloroethene Hydrodechlorination in Water by Highly*
520 *Disordered Monometallic Nanoiron*. Chemistry of Materials, 2005. **17**(21): p.
521 5315-5322.
- 522 20. Sun, Y.-P., et al., *Characterization of zero-valent iron nanoparticles*.
523 *Advances in Colloid and Interface Science*, 2006. **120**(1-3): p. 47-56.
- 524 21. Chen, L.-H., C.-C. Huang, and H.-L. Lien, *Bimetallic iron-aluminum particles*
525 *for dechlorination of carbon tetrachloride*. Chemosphere, 2008. **73**(5): p. 692-
526 697.
- 527 22. Frost, R.L., G.A. Cash, and J.T. Kloprogge, [*']Rocky Mountain leather'*,
528 *sepiolite and attapulgite--an infrared emission spectroscopic study*.
529 *Vibrational Spectroscopy*, 1998. **16**(2): p. 173-184.
- 530 23. Frost, R.L., et al., *Near-infrared and mid-infrared spectroscopic study of*
531 *sepiolites and palygorskites*. *Vibrational Spectroscopy*, 2001. **27**(1): p. 1-13.
- 532 24. McKeown, D.A., J.E. Post, and E.S. Etz, *Vibrational analysis of palygorskite*
533 *and sepiolite*. Clays Clay Miner. FIELD Full Journal Title:Clays and Clay
534 Minerals, 2002. **50**(5): p. 667-680.
- 535 25. Suarez, M. and E. Garcia-Romero, *FTIR spectroscopic study of palygorskite:*
536 *Influence of the composition of the octahedral sheet*. Applied Clay Science,
537 2006. **31**(1-2): p. 154-163.
- 538 26. Augsburger, M.S., et al., *FTIR and Mossbauer investigation of a substituted*
539 *palygorskite: Silicate with a channel structure*. Journal of Physics and
540 Chemistry of Solids, 1998. **59**(2): p. 175-180.
- 541 27. Chahi, A., S. Petit, and A. Decarreau, *Infrared evidence of dioctahedral-*
542 *trioctahedral site occupancy in palygorskite*. Clays and Clay Minerals, 2002.
543 **50**(3): p. 306-313.
- 544 28. Madejova, J. and P. Komadel, *Baseline studies of the Clay Minerals Society*
545 *source clays: infrared methods*. Clays and Clay Minerals, 2001. **49**(5): p. 410-
546 432.

- 547 29. Mendelovici, E. and D.C. Portillo, *Organic derivatives of attapulgite. I.*
548 *Infrared spectroscopy and x-ray diffraction studies.* Clays and Clay Minerals,
549 Proceedings of the Conference, 1976. **24**(4): p. 177-82.
- 550 30. Blanco, C., et al., *Differences between one aluminic palygorskite and another*
551 *magnesian by infrared spectroscopy.* Spectroscopy Letters, 1989. **22**(6): p. 659-
552 73.
- 553 31. Wang, W., H. Chen, and A. Wang, *Adsorption characteristics of Cd(II) from*
554 *aqueous solution onto activated palygorskite.* Separation and Purification
555 Technology, 2007. **55**(2): p. 157-164.
- 556 32. Jozefaciuk, G. and G. Bowanko, *Effect of acid and alkali treatments on*
557 *surface areas and adsorption energies of selected minerals.* Clays and Clay
558 Minerals, 2002. **50**(6): p. 771-783.
- 559 33. Neaman, A. and A. Singer, *Rheological properties of aqueous suspensions of*
560 *palygorskite.* Soil Science Society of America Journal, 2000. **64**(1): p. 427-
561 436.
- 562 34. Cagatay, M.N., *Palygorskite in the Eocene rocks of the Dammam Dome, Saudi*
563 *Arabia.* Clays and Clay Minerals, 1990. **38**(3): p. 299-307.
- 564 35. Soong, R., *Palygorskite occurrence in northwest Nelson, South Island, New*
565 *Zealand.* New Zealand Journal of Geology and Geophysics, 1992. **35**(3): p.
566 325-30.
- 567 36. Noubactep, C., *A critical review on the process of contaminant removal in*
568 *Fe₀-H₂O systems.* Environmental Technology, 2008. **29**(8): p. 909-920.

569
570
571
572
573
574
575
576
577
578
579
580

581 **List of figures**

582

583 Fig. 1a XRD patterns of untreated/acid treated palygorskites

584 Fig. 1b XRD patterns of lab made ZVI and ZVI from Sigma

585 Fig. 1c XRD patterns of ZVI grafted on untreated/acid treated palygorskites

586

587 Fig. 2a FTIR spectrum of untreated/acid treated palygorskites (3800 to 2800 cm^{-1})

588 Fig. 2b FTIR spectrum of ZVI grafted untreated/acid treated palygorskites (3800 to
589 2800 cm^{-1})

590 Fig. 3a FTIR spectrum of untreated/acid treated PF1-1 palygorskites (1700 to
591 1300 cm^{-1})

592 Fig. 3b FTIR spectrum of ZVI grafted untreated/acid treated PF1-1 palygorskites
593 (1700 to 1300 cm^{-1})

594

595 Fig. 4a FTIR spectrum of untreated/acid treated PF1-1 palygorskites (1300 to 600 cm^{-1})

596 Fig. 4b FTIR spectrum of ZVI grafted on untreated/acid treated PF1-1 palygorskites
597 (1300 to 600 cm^{-1})

598

599 Fig. 5 SEM images of a: untreated PF1-1 palygorskite; b: 5M HCl treated
600 palygorskite; c: ZVI from Sigma; d: laboratory made ZVI; e: ZVI grafted on
601 treated palygorskite and f: ZVI grafted on untreated palygorskite

602

603 Fig. 6 EDX mapping and element analysis on ZVI grafted palygorskite a: SEM image;
604 b: C element distribution; c: Si element distribution; d: O element distribution;
605 e: Fe element distribution and f: EDX spectrum of selected area

606

607 Fig. 7 TEM image of laboratory made ZVI particles

608

609 Fig. 8 Effect of mixing time on MB removal

610

611

612

613

614

615

616